NOTES AND CORRESPONDENCE

Dissipative Losses in Nonlinear Internal Waves Propagating across the Continental Shelf

J. N. MOUM

College of Oceanic and Atmospheric Sciences, Oregon State University, Corvallis, Oregon

D. M. FARMER

Graduate School of Oceanography, University of Rhode Island, Kingston, Rhode Island

E. L. SHROYER AND W. D. SMYTH

College of Oceanic and Atmospheric Sciences, Oregon State University, Corvallis, Oregon

L. ARMI

Scripps Institution of Oceanography, La Jolla, California

(Manuscript received 17 July 2006, in final form 31 October 2006)

ABSTRACT

A single nonlinear internal wave tracked more than 100 wavelengths across Oregon's continental shelf over a 12-h period exhibited nearly constant wave speed, $c = 0.75$ m s^{-1}, and amplitude, $a = 15$ m. The wavelength L gradually decreased from 220 m in 170-m water depth to 60 m in 70-m water depth. As the water shallowed beyond 50 m, the wave became unrecognizable as such. The total energy decreased from 1.1 to 0.5 MJ m^{-1}. The rate at which wave energy was lost, $-dE/dt = 14$ [7, 22] W m^{-1}, was approximately equal to the energy lost to turbulence dissipation, $\rho\varepsilon = 10$ [7, 14] W m^{-1}, as inferred from turbulence measurements in the wave cores plus estimates in the wave-induced bottom boundary layer. The approximate balance, $dE/dt = -\rho\varepsilon$, differs from the solibore model of Henyey and Hoering in which the potential energy across the wave balances $\rho\varepsilon$. However, other evidence suggests that the wave evolved from a solibore-like state to a dissipative solitary wavelike state over the observed propagation path.

1. Introduction

The evolution of energy in a two-dimensional, nonhydrostatic, nonlinear internal wave is governed by

$$\frac{\partial E}{\partial t} + \frac{\partial f_E}{\partial x} + \text{vertical redistribution} = -\rho\varepsilon + \text{other sources/sinks}, \quad (1)$$

where E is the sum of kinetic (KE $= \frac{1}{2}\rho u_i u_i$) plus available potential energy (APE), ρ is density, ε is the rate of energy lost to turbulence, and f_E is the horizontal energy flux. The energy flux in nonlinear waves includes significant contributions from nonlinear advection and nonhydrostatic pressure–velocity work, providing a clear distinction from linear internal waves (Moum et al. 2007). Vertical redistribution does not affect the energy when averaged laterally and vertically over the wave.

Aside from turbulence losses, another possible energy sink is the generation of small-scale internal waves by the wave disturbance, as has been observed in atmospheric flows of similar form (Crook 1988). More relevant here is the prospect of a wave potential energy source in the form of an asymmetry in the density structure across the waves. This essentially defines the distinction between solibores (Henyey and Hoering

Corresponding author address: J. N. Moum, College of Oceanic and Atmospheric Sciences, Oregon State University, COAS Admin. Bldg. 104, Corvallis, OR 97331-5503.
E-mail: moum@coas.oregonstate.edu

DOI: 10.1175/JPO3091.1

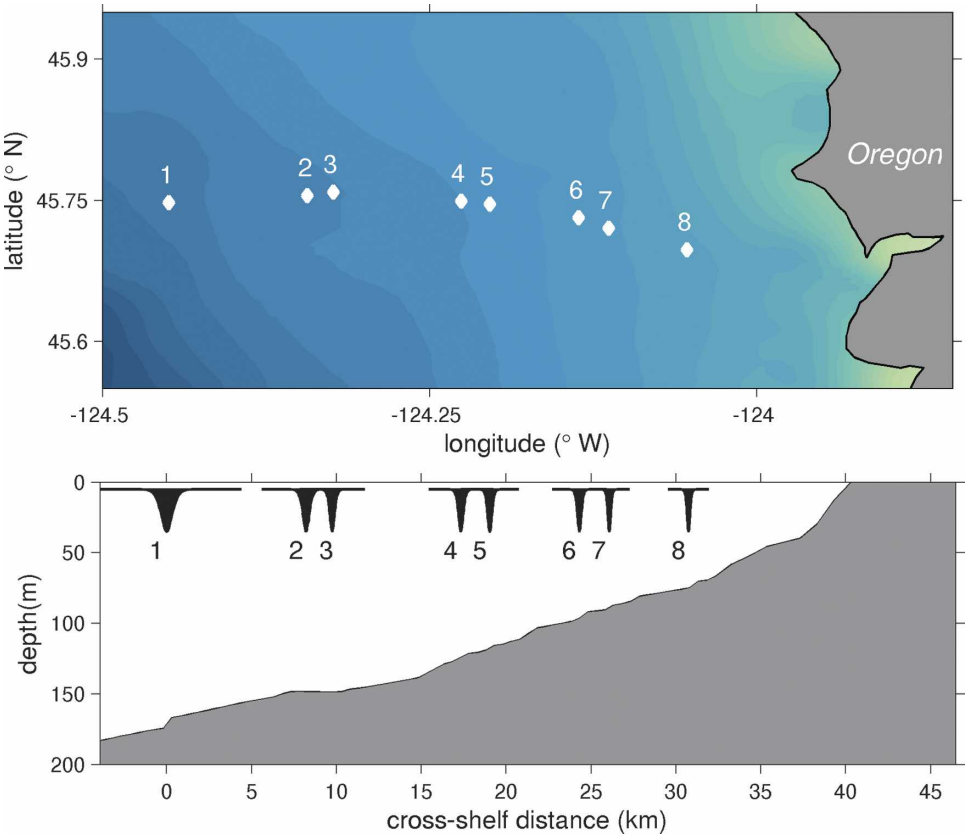

FIG. 1. Nonlinear internal wave observations across the shelf. (top) Locations of each sighting where detailed profiling observations were made. (bottom) Bottom depth along ship track. Shown schematically are waveforms indicating relative wave amplitudes (×2) and wavelengths (×2) as determined from our observations.

1997) and purely solitary waves. Both asymmetric (Farmer and Smith 1980; Wesson and Gregg 1994)[1] and symmetric (Stanton and Ostrovsky 1998; Nash and Moum 2005) forms have been observed. In the solibore case, Henyey and Hoering (1997) argue that the wave is in steady state, the potential energy supplied by the asymmetric stratification in balance with $-\rho\varepsilon$. In the solitary wave case, no external energy supply exists, and $dE/dt = -\rho\varepsilon$. In this case, dissipation must diminish wave energy, and one of our goals is to quantify this. Over sufficiently short times, however, dissipative effects are negligible and the wave may be considered freely propagating. We consider the distinction between solibores and solitary waves in terms of the evolution of an individual wave propagating onto the continental shelf (Fig. 1). In particular, we follow the leading wave of a train of nonlinear internal waves over a distance of about 30 km in a 12-h period.

For linear internal waves, it is straightforward to show that $f_E = cE$ (Kundu and Cohen 2004). This equality has been verified experimentally for nonlinear internal waves by Moum et al. (2007) over a short propagation range (i.e., on the order of a wavelength). For it to be true, the role of dissipative losses ($-\rho\varepsilon$) must be small.[2] Observations of nonlinear internal waves propagating through deep water suggest that they are only weakly turbulent, both at the equator (Pinkel 2000) and in the South China Sea (Chang et al. 2006; Klymak et al. 2006). However, this is not the case for waves observed propagating over the continental shelf (Moum et al. 2003). Does turbulence contribute significant losses to the propagation of wave energy

[1] These two examples were used by Henyey and Hoering (1997) as case studies to compare estimates of the potential energy supplied by the bore to the wave and dissipative losses within the wave.

[2] At any location, $\partial E/\partial t = -\partial f_E/\partial x - \rho\varepsilon$. If the wave propagates at speed c without change of form, $\partial E/\partial t = -c\partial E/\partial x$. If $\rho\varepsilon$ is negligible, these two equations may be combined and integrated to yield $f_E = cE$.

over long ranges (100 s of wavelengths) in relatively shallow water?

2. Experiment

On 28 June 2000, we encountered a well-formed train of nonlinear internal waves propagating shoreward in 170-m water depth 40 km offshore of Cape Falcon, Oregon (Fig. 1). Using a high-frequency echosounder (120 kHz), acoustic Doppler current profiler (ADCP; 300 kHz), and Chameleon turbulence profiler (Moum et al. 1995), we repeatedly made transits across the leading wave as it propagated 32.5 km onshore over a period of 12 h. During this period a sequence of sampling patterns was repeated. An upstream density profile was obtained, and the wave was crossed at 6–8 kt perpendicular to the wave front (as determined from visual and radar observation) to define its spatial structure by acoustic imaging (Fig. 2). We then drifted and profiled with Chameleon before and as the wave passed the ship; this resulted in many profiles through the waves, but as the ship was carried by the large wave currents, presented a distorted view of the wave's structure. A repeat crossing at 6–8 kt across the wave front followed immediately. As the water shallowed, the form of the wave became less recognizable, and the final crossing shown in Fig. 2 was the last transit of the wave where we could clearly identify a wavelike structure.

3. Calculation of wave energies

In all but the first transect of the wave, ADCP velocity measurements were too coarsely resolved (at 30-s ensemble averages) to provide a useful estimate of wave kinetic energy. Instead, we estimate KE indirectly. These estimates require the following assumptions:

1) In the wave's reference frame, streamlines are parallel to isopycnals. This is true if the wave is two-dimensional and mixing effects are small enough that there is no significant change of form in the time required to pass a fixed point (although mixing is significant over longer times).
2) Isopycnal (and streamline) displacements have the form

$$\eta(x, z, t) = a\phi(z)\,\mathrm{sech}^2\frac{x'}{L}. \qquad (2)$$

Here, η is a vertical displacement function with amplitude a and vertical structure function ϕ. The constant L is a length scale, and $x' = x - ct$ is the horizontal coordinate in the wave reference frame, which translates to the right at speed c with respect to the earth coordinate x.

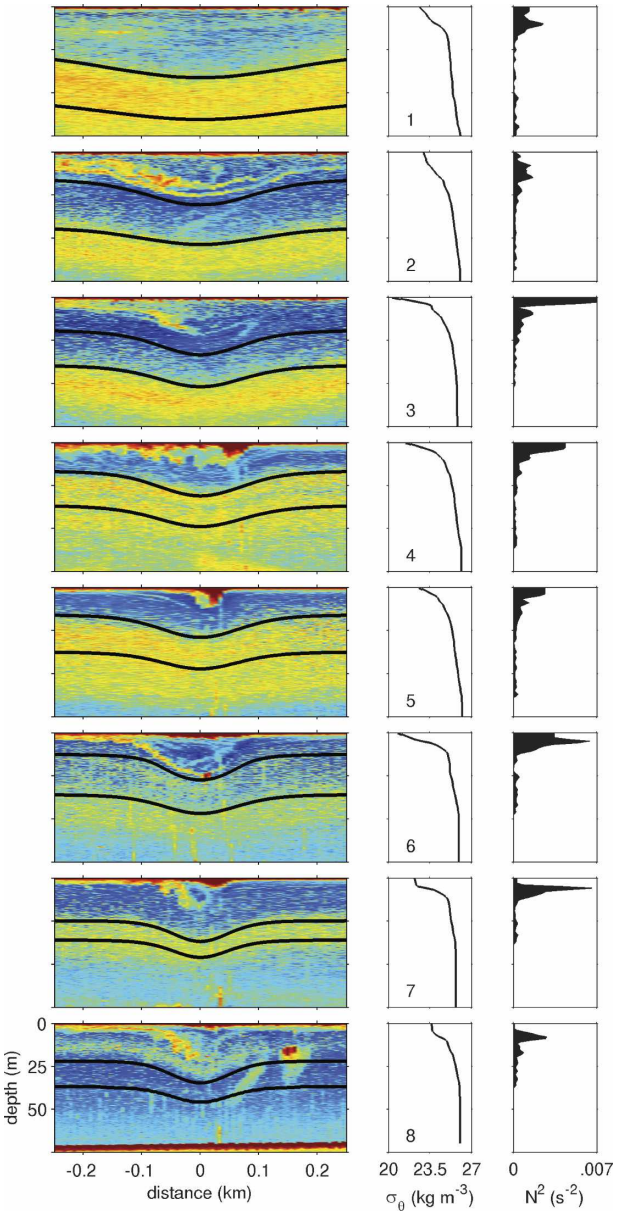

FIG. 2. Profiles of σ_θ and N^2 obtained immediately ahead of the acoustic images (120-kHz echosounder) taken at each sighting. On the acoustic images are plotted isopycnals estimated from the density profiles shown and predictions as described in the text. Each of these acoustic measurements was made while transiting in a direction perpendicular to the wave fronts at a speed much greater than the wave speed, thus minimizing the distortion of the wave shape. In this representation, the waves propagate from left to right. The seafloor appears in the acoustic image of the final wave transit.

The displacement structure function ϕ is estimated by comparing the density profile upstream of the wave and that measured as close as possible to the wave

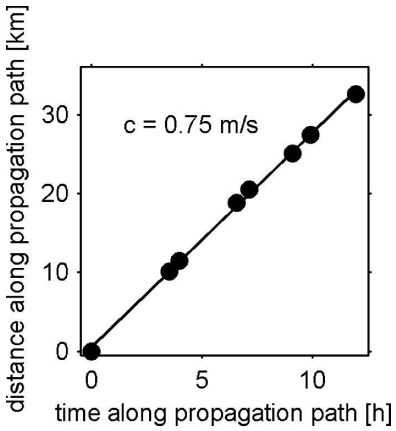

FIG. 3. Relative time vs relative position of wave sightings along the wave's propagation path. The slope of this line is the wave speed c.

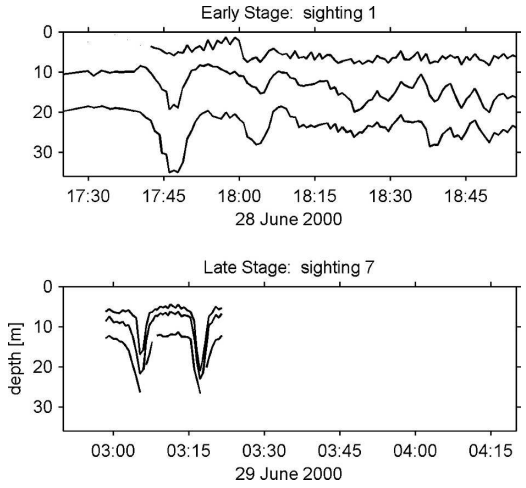

FIG. 4. Two examples of wave structure, as outlined by isopycnals measured with ship drifting and waves propagating past. Each record is 1.5 h long. (top) The early stage structure (wave sighting 1) and (bottom) a later stage (wave sighting 7). While the early stage suggests a borelike structure in which isopycnals are depressed in the wave's lee, the later stage suggests symmetry of the isopycnals across the wave, a more solitary wave–like structure.

trough. The resulting displacement profile is smoothed using a 5-m double boxcar filter to remove effects of small-scale motions. This displacement profile provides only a lower bound on the wave amplitude, since it is never measured exactly at the wave trough. Therefore, we normalize the profile so that its maximum absolute value is unity, then obtain the amplitude a via a visual fit to the echosounder image. The length scale L is also obtained by fitting to the echosounder image. The wave speed c is determined from the slope of the wave's position relative to its travel time (Fig. 3).

Having estimated $\eta\ (x, z, t)$, it is straightforward to extrapolate the density and streamfunction fields from their upstream profiles. The upstream density profile is measured, while the upstream streamfunction is just cz. The streamfunction is then transformed into the earth's reference frame, and the velocity field computed by differentiation.

At site 1, the wave was broad and background velocities were weak, permitting an independent estimate of $\langle \mathrm{KE} \rangle$ ($\langle\,\rangle = \int_{-\infty}^{\infty} \int_{0}^{H} (\,)\, dz\, dx$), determined directly from ADCP measurements. The results from the two crossings, made before and after profiling, agreed within 28% and 1%, respectively, of that predicted by the method described above. It is important to note that the directly measured background KE (in the plane of wave propagation) is an order of magnitude smaller than the wave KE.

APE was determined using the isopycnals inferred by the procedure described above and following the method outlined by Moum et al. (2007), in which the wave-induced density anomaly is defined by referencing the wave to a thermodynamic rest state (Hebert 1988; Winters et al. 1995).

We note here that the operator $\langle\,\rangle$ defines a horizontal integration over the leading wave of the wave train only. The limits $\pm\infty$ are artificial in the sense that we have constructed symmetric density and streamfunction fields. While the KE density is 0 outside of the wave, APE density is not. Although it is small, the integrated contribution is critical to a correct determination of $\langle \mathrm{APE} \rangle$ (Hebert 1988).

4. Wave properties

a. Evolution along the propagation path

The observed propagation range of 32.5 km is equivalent to >100 wavelengths. A considerable difference in the density structure was observed along the wave propagation path. Since the depression of scattering layers accurately represents that of isopycnals, at least over a wavelength (Moum et al. 2003), then the acoustic images in Fig. 2 suggest that a was approximately constant at 14–16-m displacement. Our observations also indicate that the mean speed of 0.75 m s^{-1} over the observation period is representative throughout (Fig. 3).

Two significant structural changes occur as the wave propagates onshore. The first is the reduction in L. This is depicted schematically in the second panel of Fig. 1; L decreased from 220 m at the first sighting to 60 m at the final sighting. The second change is from an apparently asymmetric density structure at the early stages of the wave's evolution (upper panel, Fig. 4) to a symmetric density structure across the wave at later stages

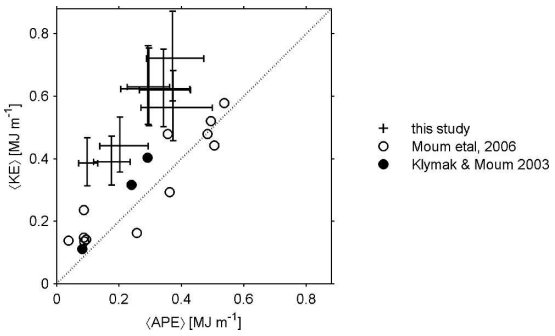

FIG. 5. Comparison of wave kinetic and available potential energy; units are per unit alongshore distance. The crosses represent estimates for the depression waves shown in Fig. 2. Uncertainties were assessed by computing ⟨KE⟩ and ⟨APE⟩ using our best estimate of $\eta \pm 10\%$. This has a significantly greater effect than a 20% variation in L. Closed circles are predictions for elevation waves over the Oregon shelf; open circles represent directly measured energies of elevation waves over the Oregon shelf. Although not shown here, the values for observed South China Sea waves follow the same line, but are larger by a factor of 10^3.

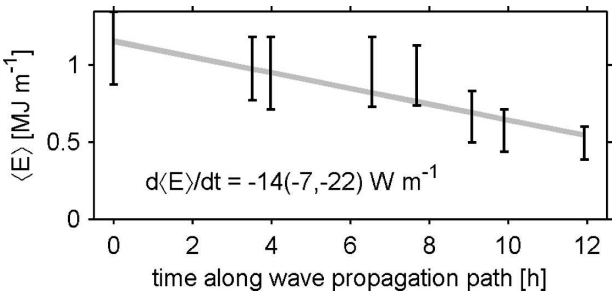

FIG. 6. Wave energy (per unit along-shelf distance), KE + APE, as a function of time along the wave propagation path. Confidence limits indicate the range determined using $\eta \pm 10\%$. The mean slope (with uncertainties) is indicated.

(lower panel, Fig. 4). The upper panel is similar in nature to the depictions of solibores reproduced by Henyey and Hoering (1997). However, while the density structure is asymmetric over several waves, the structure across the leading wave appears to be nearly symmetric, as if the leading wave is in the process of leaving the solibore. The lower panel indicates a density structure that is not at all borelike.

b. Energetics

The ⟨KE⟩ and ⟨APE⟩ range from about 0.2 to 0.8 megajoule per meter of along-wave-axis distance (roughly alongshore or north–south; Fig. 5). The ratio $\langle KE\rangle/\langle APE\rangle \simeq 2$ (95% confidence limits [1.6, 2.3]) is somewhat larger than the value 1.4 found in predicted fields determined for the bottom-trapped waves observed by Klymak and Moum (2003) and the surface-trapped South China Sea waves observed by Klymak et al. (2006). (South China Sea energies are larger by a factor of 10^3 and are not shown in Fig. 5.) This ratio differs again from that determined from direct and well-resolved measurements of bottom-trapped elevation waves by Moum et al. (2007), which indicate the energy is more closely equipartitioned between kinetic and potential energy (open dots in Fig. 5).

The total wave energy $\langle E\rangle$ decreased by about a factor of 2, from 1.1 to 0.5 MJ m^{-1} along the wave's propagation path, although not linearly (Fig. 6). The mean rate of decrease was $d\langle E\rangle/dt = -14$ [-7, -22] W m^{-1}.

c. Dissipative losses

Our investigation of turbulence generation in nonlinear internal waves over the continental shelf (Moum et al. 2003) suggest that high mode compressive wave straining acts to locally enhance shear near the wave trough. This can create explosively growing small-scale shear instabilities that break and cause turbulence along the trailing edges of the waves. A consequence is the bright acoustic scattering layers often observed along the trailing edges of waves. It is also possible that larger, more slowly growing instabilities can form within the wave core [such as seen in Moum et al.'s (2003) Fig. 14] and that the ultimate demise of these will result in a completely turbulent wave core. An example is shown in Fig. 7; this is the most highly turbulent example.

Similar profiling density was conducted through each of the eight sightings of the wave. The spatial integral $\langle\rho\varepsilon\rangle$ was approximated by multiplying the average value of $\rho\varepsilon$ in the wave core by the wave area, $\int_{-\infty}^{\infty} a\,\mathrm{sech}^2(x'/L)\,dx = 2aL$ (Fig. 8; black dots). The wave also loses energy through its interaction with the bottom, which we did not measure directly. This energy loss was approximated using the wave's near-bottom velocity applied to a law of the wall, $\varepsilon = u_*^3/(\kappa z)$, where $\kappa = 0.4$ and the friction velocity, u_*, was determined from the predicted velocity applied to a neutrally stratified bottom boundary layer of 5-m depth (Fig. 5; gray dots). This method is described by Perlin et al. (2005).

The sum of $\langle\rho\varepsilon\rangle_{\text{surface}} + \langle\rho\varepsilon\rangle_{\text{bottom}}$ along the wave's propagation path varied from 3 to 45 W m^{-1}, the surface layer generally dominating. The largest values occurred near 17 km, where the bottom slope changed. The mean value of 10 W m^{-1} (95% confidence limits [8, 14]) is within the range estimated for the loss rate of total wave energy shown in Fig. 6.

5. Summary and discussion

A single wave was tracked for more than 100 wavelengths as it propagated shoreward over the continental shelf for a 12-h period. While the wavelength decreased

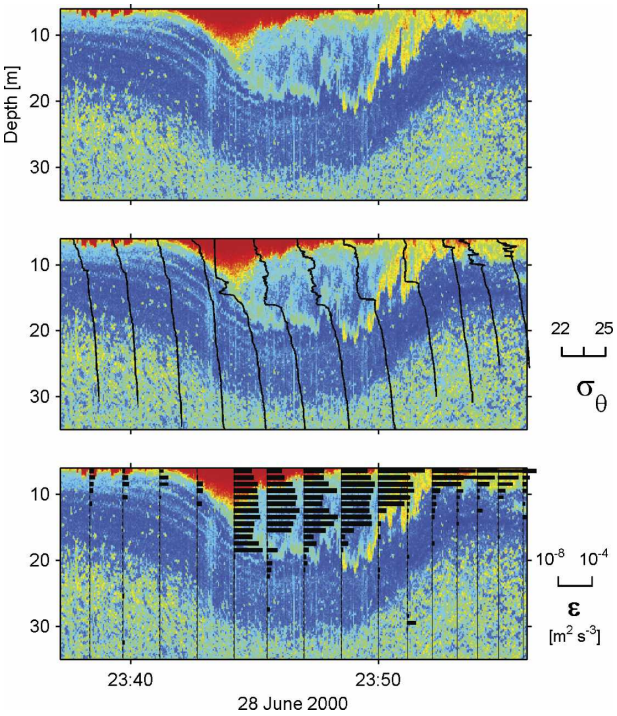

FIG. 7. Acoustic image of the wave at location 4 (refer to Fig. 2) while drifting and profiling through the wave. Because the wave shape is distorted, it is presented as a time series. The leading edge of the wave appears at 2343 UTC. The trailing edge of the wave is highly turbulent. Plotted over the middle image are profiles of σ_θ. Plotted over the lower image are profiles of ε. Profile times coincide with the lower limit of the ε plots.

significantly, the wave speed and amplitude were nearly constant. The rate at which energy was observed to be lost along the wave's propagation path was nearly equal to that observed to be lost to turbulence dissipation.

The symbols shown in Fig. 1 represent only the times that we profiled through the waves. However, we crossed the wave packet many other times, using solely acoustic methods of detection. As the wave train propagated toward shore, the spacing between waves changed continually. While it is possible that unobserved wave interactions have created an ambiguity in our interpretation, we observed no indication of direct interaction between waves.

The ultimate demise of the waves is apparently catastrophic and unclear. However, at some point we can no longer consider these to be simple nonlinear internal waves. Inshore of 50-m water depth, the wave lost its wavelike characteristics. Whether a conversion from depression waves to elevation waves occurs cannot be determined from our observations.

We have made a single estimate for the rate at which energy is lost by the wave; this loss rate does not necessarily appear to be constant (Fig. 6), and nor does $\langle \rho\varepsilon \rangle$

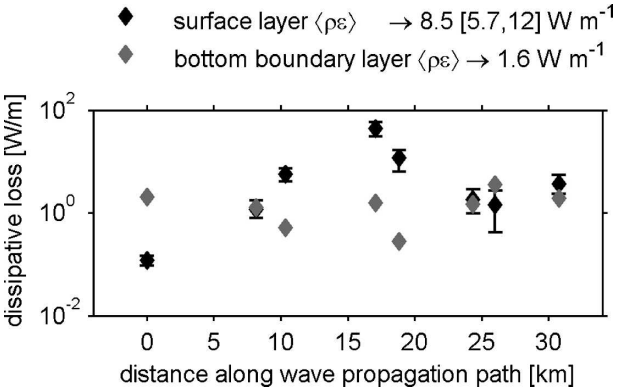

FIG. 8. Energy dissipated by turbulence (per unit along-shelf distance) as a function of distance along the wave propagation path. The surface layer values were averaged over the observed profiles and integrated over the wave (95% bootstrapped confidence limits shown). The bottom boundary layer values were estimated using a law of the wall applied to the bottom layer and a prediction of near-bottom velocity.

(Fig. 8). It is over the full extent of the observations that the balance appears to hold. It is possible that the intermittent nature of the turbulence generation process makes it difficult to assess dissipative losses without truly continuous measurements. It is also possible that our rather large uncertainties in energies mask the tendencies. But it is also possible that there is a fundamental alteration to the energetics as the wave evolves. Notably, the greatest decrease in energy occurs just past the fifth wave sighting (Fig. 6), which immediately follows the largest dissipative losses (Fig. 8). It is consistent with the early stage structure (upper panel, Fig. 4) that the initial balance is solibore-like, potential energy supply $= -\rho\varepsilon$, and $dE/dt = 0$. The late stage structure (lower panel, Fig. 4) is similarly consistent with a freely propagating solitary wave. This final possibility suggests that we did not observe an important intermediate step in which the solitary wave departed from the bore, a step we imagine to be similar to the fission process observed by Nash and Moum (2005).

Acknowledgments. The bulk of this work was funded by the Office of Naval Research. E. Shroyer and W. Smyth were supported by the National Science Foundation (Grants 9819531, 0453140). We are grateful to captain and crew of R/V *Wecoma* for their help and to Ray Kreth, Greig Thompson, Mike Neeley-Brown, and Rita Brown for their technical expertise. Thanks are given to Jonathan Nash, Alexander Perlin, and Greg Avicola for comments on an early draft.

REFERENCES

Chang, M.-H., R.-C. Lein, T. Y. Tang, E. A. D'Asaro, and Y. J. Yang, 2006: Energy flux of nonlinear internal waves in north-

ern South China Sea. *Geophys. Res. Lett.,* **33,** L03607, doi:10.1029/2005GL025196.

Crook, N. A., 1988: Trapping of low-level internal gravity waves. *J. Atmos. Sci.,* **45,** 1533–1541.

Farmer, D. M., and J. D. Smith, 1980: Tidal interaction of stratified flow with a sill in Knight Inlet. *Deep-Sea Res.,* **27A,** 239–245.

Hebert, D., 1988: The available potential energy of an isolated feature. *J. Geophys. Res.,* **93,** 556–564.

Henyey, F. S., and A. Hoering, 1997: Energetics of borelike internal waves. *J. Geophys. Res.,* **102,** 3323–3330.

Klymak, J. M., and J. N. Moum, 2003: Internal solitary waves of elevation advancing on a shoaling shelf. *Geophys. Res. Lett.,* **30,** 2045, doi:10.1029/2003GL017706.

——, R. Pinkel, C.-T. Liu, A. K. Liu, and L. David, 2006: Prototypical solitons in the South China Sea. *Geophys. Res. Lett.,* **33,** L11607, doi:10.1029/2006GL025932.

Kundu, P. K., and I. M. Cohen, 2004: *Fluid Mechanics.* 3d ed. Elsevier Academic, 759 pp.

Moum, J. N., M. C. Gregg, R. C. Lien, and M. Carr, 1995: Comparison of turbulence kinetic energy dissipation rate estimates from two ocean microstructure profilers. *J. Atmos. Oceanic Technol.,* **12,** 346–366.

——, D. M. Farmer, W. D. Smyth, L. Armi, and S. Vagle, 2003: Structure and generation of turbulence at interfaces strained by internal solitary waves propagating shoreward over the continental shelf. *J. Phys. Oceanogr.,* **33,** 2093–2112.

——, J. M. Klymak, J. D. Nash, A. Perlin, and W. D. Smyth, 2007: Energy transport by nonlinear internal waves. *J. Phys. Oceanogr.,* **37,** 1968–1988.

Nash, J. D., and J. N. Moum, 2005: River plumes as a source of large amplitude internal waves in the ocean. *Nature,* **437,** 400–403.

Perlin, A., J. N. Moum, J. M. Klymak, M. D. Levine, T. Boyd, and P. M. Kosro, 2005: A modified law-of-the-wall to describe velocity profiles in the bottom boundary layer. *J. Geophys. Res.,* **110,** C10S10, doi:10.1029/2004JC002310.

Pinkel, R., 2000: Internal solitary waves in the warm pool of the western equatorial Pacific. *J. Phys. Oceanogr.,* **30,** 2906–2926.

Stanton, T. P., and L. A. Ostrovsky, 1998: Observations of highly nonlinear internal solitons over the continental shelf. *Geophys. Res. Lett.,* **25,** 2695–2698.

Wesson, J. C., and M. C. Gregg, 1994: Mixing at Camarinal Sill in the Strait of Gibraltar. *J. Geophys. Res.,* **99,** 9847–9878.

Winters, K. B., P. N. Lombard, J. J. Riley, and E. A. D'Asaro, 1995: Available potential energy and mixing in density-stratified fluids. *J. Fluid Mech.,* **289,** 115–128.